Online Identification Strategy of Secondary Time Constant and Magnetizing Inductance for Linear Induction Motors

Dinghao Dong, *Student Member, IEEE*, Wei Xu, *Senior Member, IEEE*, Xinyu Xiao, Yirong Tang, *Student Member, IEEE*, and Kai Yang

***Abstract*—In this article, an online dual-parameter identification strategy for linear induction motors (LIMs) is investigated. Considering the influence of unique end effects in LIMs and the critical impact on control system performance, the magnetizing inductance and secondary time constant are chosen as the targets of estimation. Compared with rotary induction motors, the influence factors in LIMs are much more complex, which can heavily affect the parameter value especially for the high-speed condition. As a result, the online identification is vital for high performance applications. Based on the model reference adaptive system with magnetizing current as state variable, this article starts from the adaptive law of secondary time constant derived by Popov's criterion for hyperstability. Then, the physical significance and stable range are analyzed in details, based on which a handy magnetizing inductance identification method is combined. To further ensure the precision of estimation, one simplification scheme is specially designed. Besides, to eliminate the pure integrator, the derivatives of magnetizing current are chosen as the state variables. Finally, the dual-parameter identification system that utilizes only one PI controller and has low coupling property is constructed. Comprehensive simulation and experiments have fully demonstrated the effectiveness and superiorities of the proposed method.**

***Index Terms*—Linear induction motors (LIMs), model reference adaptive system (MRAS), parameter identification, physical significance analysis.**

I. Introduction

THE linear induction motors (LIMs) have arisen more and more attention for the ability to accomplish the linear motion directly, which leads to the removing of intermediate gearing device [1], [2]. Besides, it also has the superiorities in radius of turning circle, grade ability, maintenance cost, and so on, which is very suitable for the high-capacity urban rail transportation applications. Accordingly, numerous researches have got great interest in this topic [3]–[5]. However, most of them require the accurate information of motor parameters, mismatching of which will heavily influence the overall performance. Unfortunately, the parameter variation in LIMs is much more complex compared with that for rotary induction motors (RIMs). First, the special structure of LIMs, such as large air gap, leads to a small value of magnetizing inductance even though compared with leakage inductance. As a result, a relatively small error in magnetizing inductance might lead to noticeable degradation of control performance. Accordingly, the accuracy requirement of identification will be higher for LIMs. Besides, some existing identification method may lose efficacy or be degraded in accuracy. Second, the existing of dynamic longitudinal end effect (LEE) has considerable influence on the dynamic change of magnetizing inductance and secondary parameters, which will vary with the speed and load condition changing. Thus, some investigations have been put forward to study the parameter identification of LIMs [6]–[12]. However, the main attention now is focused on the offline methods [6]–[8]. To be more concrete, the researches on magnetizing inductance, secondary parameters, and dual-parameter are discussed respectively as follows.

For RIMs, the magnetizing inductance is mainly affected by the saturation level. As a result, in many conditions, the offline identification and online updating with magnetizing curve will be sufficient. However, when it comes to LIMs, the end effects have turned to be another key factor. The variation of magnetizing inductance is determined by multifactors, such as speed, slip frequency, and so on, which makes it more difficult to record the offline information. So, the online identification of magnetizing inductance just reflects the challenging of parameter identification in LIMs. Taking the strategies for RIMs into account, till now, there has been some studies focusing on the online schemes for magnetizing inductance [12]–[15]. To be clearer, the properties of the existing methods are summarized as Table I. Although the pure integrator mentioned in Table I can be solved by some methods, such as low-pass filter [16] and adaptive neural integrator [17], the computation burden will increase to some extent and other problems may arise.

Manuscript received December 7, 2021; revised February 20, 2022 and April 2, 2022; accepted April 24, 2022. Date of publication April 29, 2022; date of current version June 24, 2022. This work was supported in part by the Key Research and Development Program of Sichuan Province under Grant 2021YFG0081 and in part by the Technology and Innovation Commission of Shenzhen Municipality under Grant JCYJ20190809101205546. Recommended for publication by Associate Editor J. Ye. *(Corresponding author: Wei Xu.)*

The authors are with the State Key Laboratory of Advanced Electromagnetic Engineering and Technology, School of Electrical and Electronic Engineering, Huazhong University of Science and Technology, Wuhan 430074, China (e-mail: dinghaodongee@foxmail.com; weixu@hust.edu.cn; xinyuxiao@hust.edu.cn; yirtang@foxmail.com; yk@hust.edu.cn).

Color versions of one or more figures in this article are available at https://doi.org/10.1109/TPEL.2022.3171412.

Digital Object Identifier 10.1109/TPEL.2022.3171412

TABLE I
COMPARISON BETWEEN THE EXISTING METHODS AND PROPOSED METHOD

Number	Contribution and Advantage	Disadvantage
[12]	A full-order-observer-based strategy is presented; pure integrator is avoided	The tuning of gain matrix is complex; full-range stability analysis is not given
[13]	Simple structure, ease of implementation, low parameter sensitivity	Magnetizing curve of the machine is needed
[14]	Without using magnetizing curve	One suffers from pure integral problem; one relies on the precise orientation and steady state
[15]	Without using any additional data fitting method	Flux should be varied during identification
[32]	Magnetizing inductance and rotor resistance are identified parallelly	PI gains should be properly signed for stability
[33]	Observer is robust to uncertainties in the leakage inductance values	Relatively sensitive to the stator resistance; error is high at low torque
[9]	Terminal impedance are utilized to realize the identification	Accurate terminal impedance should be calculated
[10]	Dual-parameter identification for LIM is conducted	Both state observer and thrust observer are needed; coupling is not analyzed
Proposed method	Clear physical significance; pure integrator is eliminated; only one coefficient simplification is needed; weak coupling; only one PI controller is utilized	Relatively sensitive to uncertainties in the stator resistance values; dependence on the information of rough value of magnetizing inductance

Except for the influence on magnetizing inductance, the end effects will also lead to additional eddy-current loss according to relevant research [18]–[21], which will introduce an additional resistance into LIMs model. Thus, the variation of secondary parameter in LIMs will be much more complex and severe. For rotor resistance or rotor time constant of RIMs, there have been quite a lot of literatures aimed at the online identification. The model-based methods mainly adopt the model reference adaptive system (MRAS) structure with different variables, such as rotor flux [22], derivative rotor flux [23], electromagnetic torque [24], stator voltage [25], reactive power [26], [27], and magnetizing current [28] to derive the various adaptive laws. To analyze the MRAS strategies with different functional candidates more clearly, one unified model on the basis of indirect field orientation control (FOC) for RIMs is developed in [29]. Except for the abovementioned fundamental-frequency-model-based methods, some methods conduct the identification by utilizing small signal injection [30] or ever-present signal jitter [31], which can be cooperated with the sensorless control. While, the additional signal injection or specially designed filter will increase the complexity and even degrade the performance of drive system.

For that both magnetizing inductance and secondary parameters are heavily affected by multiple factors in LIMs, the parallel identification is significant for high-performance control. However, for the difficulties, relatively less researches are aimed to solve this issue, which are also summarized in Table I. It is worth mentioning that the compensation of inverter nonlinearities is one of the key issues in parameter identification, which needs the information of excitation voltage. However, it has been deeply investigated by [34]–[37], and, in this article, it is set as one of the basic theories, just like the FOC, rather than one of the researching focuses.

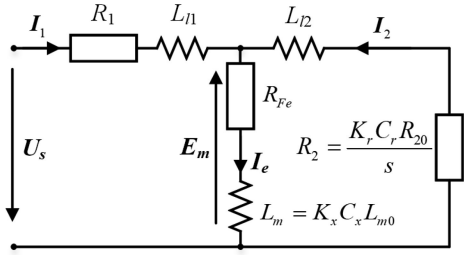

Fig. 1. T-model steady-state equivalent circuit of LIMs.

In this article, a practical strategy to identify magnetizing inductance and secondary time constant online is proposed for LIMs traction system. The particularity of LIMs is fully taken into consideration. The Popov's criterion for hyperstability is adopted to design adaptive law of secondary time constant, in which the global asymptotic stability can be ensured. And then the physical significance is revealed. On this basis, the magnetizing inductance calculation method is derived and the proposed dual-parameter identification strategy is decoupled. As a result, the overall stability of system can be analyzed easily and only one PI controller is needed to simplify the tuning process. Besides, the pure integrator is removed by adopting the derivatives of magnetizing current as the state rather than the secondary flux. In Section II, the mathematic model and parameter variation principle of LIMs are introduced briefly. In Section III, the basic adaptive law of secondary time constant is derived and the physical significance is clarified. Section IV makes full description on the characteristics of proposed dual-parameter identification. Comprehensive simulation and experiments are presented in Section V to verify the effectiveness, which includes the comparison with conventional strategy. Finally, Section VI concludes this article. To make a brief comparison, the proposed method is also listed in Table I, which will be further discussed in subsequent sections.

II. MODEL AND PRINCIPLE OF LIMS

For the special structure of LIMs, such as discontinuity of magnetic circuit, the mathematical model should be analyzed anew, which has been fully discussed in [18]–[21]. Before the quantitative change rule or identification method is researched, the model adopted should be explicit. The method proposed by Duncan attributes the influence of LEE to the variation of resistance and inductance in the magnetizing branch. However, it will increase the difficulty of control strategy and identification method design.

The equivalent circuit of LIMs selected in this article is based on the model researched in [18], as shown in Fig. 1, which is similar to that of RIMs and attributes end effects to the variation of magnetizing inductance and secondary resistance. As a result, the meanings of L_m and R_2 are distinctly different from these

for RIMs, for which equivalent variables should be named to distinguish them. The $K_{r,x}$ and $C_{r,x}$ mean the longitudinal-end-effect and transversal-edge-effect coefficients of the equivalent secondary resistance and magnetizing inductance, respectively, which reflect the effects of longitude and transverse end effects on parameters. It will not only bring convenience to transplant the high-performance control strategies from RIMs to LIMs, but also make the design of observation and identification system much easier.

The mathematic model in the stationary frame can be obtained by neglecting the iron loss resistance in magnetizing branch, which is usually adopted in control strategy design for the similarity with RIMs, as described by

$$\begin{cases} \frac{d\boldsymbol{i}_1}{dt} = -\frac{R_1L_2^2+R_2L_m^2}{\sigma L_1L_2^2}\boldsymbol{i}_1 + \frac{L_m}{\sigma L_1L_2T_2}\boldsymbol{\psi}_2 \\ \qquad -\frac{L_m}{\sigma L_1L_2}\omega_2\boldsymbol{J}\boldsymbol{\psi}_2 + \frac{1}{\sigma L_1}\boldsymbol{u}_1 \\ \frac{d\boldsymbol{\psi}_2}{dt} = \omega_2\boldsymbol{J}\boldsymbol{\psi}_2 - \frac{1}{T_2}\boldsymbol{\psi}_2 + \frac{L_m}{T_2}\boldsymbol{i}_1 \end{cases} \tag{1}$$

where subscripts 1 and 2 represent variables for the primary and secondary of the LIMs, respectively; $\boldsymbol{i}$, $\boldsymbol{u}$, and ψ are the current, voltage, and flux vectors, respectively; R represents the resistance, L the inductance, L_m the equivalent magnetizing inductance (called magnetizing inductance for short), R_2 the equivalent secondary resistant (called secondary resistant for short), $T_2 = L_2/R_2$ the equivalent secondary time constant (called secondary time constant for short), $\sigma = 1 - L_m^2/L_1L_2$ the leakage coefficient, $\omega_2 = v\pi/\tau$ the equivalent electrical angular velocity, v the linear speed, τ the pole pitch, and $\boldsymbol{J}$= [0,−1;10].

From (1), the classic flux-based voltage and current model can be derived as

$$\begin{cases} \frac{d\boldsymbol{\psi}_2}{dt} = \frac{L_2}{L_m}[\boldsymbol{u}_1 - (R_1\boldsymbol{i}_1 + \sigma L_1\frac{d\boldsymbol{i}_1}{dt})] \\ \frac{d\boldsymbol{\psi}_2}{dt} = \omega_2\boldsymbol{J}\boldsymbol{\psi}_2 - \frac{1}{T_2}\boldsymbol{\psi}_2 + \frac{L_m}{T_2}\boldsymbol{i}_1. \end{cases} \tag{2}$$

To separate magnetizing inductance and secondary time constant in voltage and current model, the magnetizing current is defined as

$$\boldsymbol{i_m} = \boldsymbol{\psi}_2/L_m. \tag{3}$$

On the basis of (2) and (3), the corresponding voltage and current equations for magnetizing current estimation can be arranged, respectively, as

$$\frac{d\boldsymbol{i_m}}{dt} = \frac{L_2}{L_m^2}\left[\boldsymbol{u}_1 - \left(R_1\boldsymbol{i_1} + \sigma L_1\frac{d\boldsymbol{i_1}}{dt}\right)\right] \tag{4}$$

$$\frac{d\boldsymbol{i_m}}{dt} = \omega_2\boldsymbol{J}\boldsymbol{i_m} - \frac{1}{T_2}\boldsymbol{i_m} + \frac{1}{T_2}\boldsymbol{i}_1. \tag{5}$$

Despite that the equation of secondary time constant contains the magnetizing inductance, it can be seen as one integrated independent parameter. After the magnetizing inductance and secondary time constant is estimated successfully, the secondary resistance can be calculated easily. In this way, the magnetizing inductance and secondary time constant only exist in voltage model (4) and current model (5), respectively. Selecting secondary time constant as one of the identified variables will be helpful for decoupling. That is to say, there contains no secondary resistance in (4) and no isolated magnetizing inductance in (5). Hence, the given voltage model (4) can be assigned as reference model and current model (5) as the adaptive model when the adaptive law of secondary time constant is designed. For magnetizing inductance, it will be just the reverse. The corresponding inverse-Γ equivalent circuit can be drawn as Fig. 2.

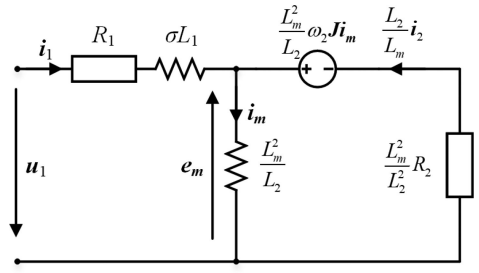

Fig. 2. Inverse-Γ dynamic equivalent circuit of LIMs.

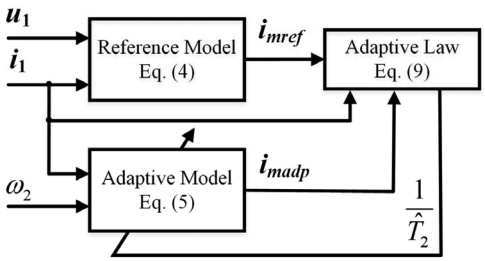

Fig. 3. Identification structure of secondary time constant based on MRAS.

Although the model introduced previously is similar to that of RIMs, the change mechanisms of some parameters are distinctly different. The additional influence factors are speed and slip frequency. Taking the end effects into consideration of parameter change, the analytical calculation formulas of them have been derived in [18], which starts from the design of LIMs and needs the knowledge of many structure parameters. The detailed expression is omitted here for the page limitation. To be more practical for realizing in control strategies, the parameters can be refreshed by the LEE factor $f(Q)$ proposed by [19], in which only some electric parameters and basic structure parameters are required. However, it is noted that the change rule of parameters should be cooperated with the adopted model for that the meaning of some parameters can be different. Besides, all of the magnetic saturation, skin effect and temperature rise are not considered in the updating formulas mentioned above, which also play a non-negligible role just like these in RIMs. As a result, it is quite difficult to consider all of the factors, respectively, and then acquire the accurate value of parameters by offline identification or theoretical calculation for LIMs. Hence, the online parameter identification is a key technology for computing all of the influence factors roundly.

III. Identification of Secondary Time Constant

A. Adaptive Law Derivation

According to (4) and (5), the secondary time constant can be identified by constructing MRAS system, as shown in Fig. 3, with the assumption that magnetizing inductance is known.

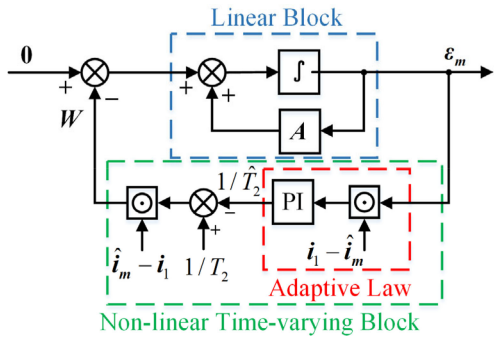

Fig. 4. Equivalent nonlinear feedback system.

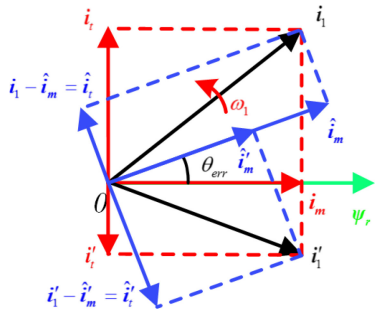

Fig. 5. Phasor diagram of $\boldsymbol{i_m}$ and $\boldsymbol{i_1} - \boldsymbol{i_m}$ at steady state.

The adaptive mechanism can be designed by the Popov's criterion for hyperstability. The estimation equation can be derived from (5) as

$$\frac{d\hat{\boldsymbol{i}}_{\boldsymbol{m}}}{dt} = \omega_2 \boldsymbol{J}\hat{\boldsymbol{i}}_{\boldsymbol{m}} - \frac{1}{\hat{T}_2}\hat{\boldsymbol{i}}_{\boldsymbol{m}} + \frac{1}{\hat{T}_2}\boldsymbol{i}_1. \tag{6}$$

Furtherly, the state error equation of magnetizing current can be deduced as

$$\frac{d\boldsymbol{\varepsilon_m}}{dt} = \omega_2 \boldsymbol{J}\boldsymbol{\varepsilon_m} - \frac{1}{T_2}\boldsymbol{\varepsilon_m} - \left(\frac{1}{T_2} - \frac{1}{\hat{T}_2}\right)(\hat{\boldsymbol{i}}_{\boldsymbol{m}} - \boldsymbol{i}_1) \tag{7}$$

where $\boldsymbol{\varepsilon_m} = \boldsymbol{i_m} - \hat{\boldsymbol{i}}_{\boldsymbol{m}}$, $\boldsymbol{A} = \omega_2\boldsymbol{J} - \frac{1}{T_2}\boldsymbol{I}$, and $\boldsymbol{W} = (\frac{1}{T_2} - \frac{1}{\hat{T}_2})(\hat{\boldsymbol{i}}_{\boldsymbol{m}} - \boldsymbol{i}_1)$.

The nonlinear feedback system is drawn in Fig. 4. The forward-path transfer matrix $(s\boldsymbol{I} - \boldsymbol{A})^{-1}$ has been proved to be strictly positive real. The proof is omitted here for the page limitation. Thus, the Popov's criterion for hyperstability can be satisfied only if the following inequation is true:

$$\int_0^{t_1} \boldsymbol{\varepsilon}_m^T \boldsymbol{W} dt = \int_0^{t_1} \left(\frac{1}{T_2} - \frac{1}{\hat{T}_2}\right) \boldsymbol{\varepsilon_m^T}(\hat{\boldsymbol{i}}_{\boldsymbol{m}} - \boldsymbol{i}_1)dt \geq -\gamma_0^2$$

for all $t_1 \geq 0$. (8)

The adaptive mechanism can be designed as [28]

$$\frac{1}{\hat{T}_2} = \left(K_p + \frac{1}{s}K_i\right)\Delta\eta = \left(K_p + \frac{1}{s}K_i\right)\boldsymbol{\varepsilon_m^T}(\boldsymbol{i}_1 - \hat{\boldsymbol{i}}_{\boldsymbol{m}}). \tag{9}$$

Substituting (9) into (8), it is derived that

$$\begin{aligned}\int_0^{t_1} \boldsymbol{\varepsilon^T W} dt &= \int_0^{t_1} \left[\frac{R_2}{L_m} + \left(K_p + \frac{1}{s}K_i\right)\Delta\eta\right]\Delta\eta dt \\ &= \int_0^{t_1} \left[K_p(\Delta\eta)^2 + \left(\frac{R_2}{L_m} + \frac{K_i}{s}\Delta\eta\right)\Delta\eta\right] dt.\end{aligned} \tag{10}$$

Considering (10) and $\int_0^{t_1} \frac{df(t)}{dt} f(t)dt \geq -\frac{1}{2}f^2(0)$, it can be proved that the inequation (8) is fully satisfied. Thus, the global asymptotic stability of the system is ensured by the adaptive law (9).

B. Physical Significance Revelation

Despite that the adaptive law of secondary time constant has been obtained, the physical significance is not so clear. Besides, the reference value of magnetizing current is acquired by (4), in which the magnetizing inductance is contained. So, it is uncertain whether the deviation of magnetizing inductance will affect the accuracy of identified secondary time constant. To clarify the deep meaning of (9) and decouple the followed dual-parameter identification, the physical significance analysis is needed. More details are summarized as follows.

First, the connotation of $\boldsymbol{i}_1 - \hat{\boldsymbol{i}}_{\boldsymbol{m}}$ is clarified. Substituting (6), it can be converted as

$$\hat{\boldsymbol{i}}_{\boldsymbol{m}}(\boldsymbol{i}_1 - \hat{\boldsymbol{i}}_{\boldsymbol{m}}) = \hat{T}_2\hat{\boldsymbol{i}}_{\boldsymbol{m}}\frac{d\hat{\boldsymbol{i}}_{\boldsymbol{m}}}{dt} - \omega_2\hat{T}_2\hat{\boldsymbol{i}}_{\boldsymbol{m}}\boldsymbol{J}\hat{\boldsymbol{i}}_{\boldsymbol{m}}. \tag{11}$$

It can be concluded from (11) that the first item is always zero at steady state as long as the observer can achieve the stable condition, which is assured by the adaptive law (9). And the second item will be always zero at any state. As a result, (11) will be always zero at steady state. So, the steady-state value of secondary time constant has no concern with $\hat{\boldsymbol{i}}_{\boldsymbol{m}}(\boldsymbol{i}_1 - \hat{\boldsymbol{i}}_{\boldsymbol{m}})$ in (9). From the aspect of phasor diagram, it means that $\hat{\boldsymbol{i}}_{\boldsymbol{m}}$ is orthometric to $\boldsymbol{i}_1 - \hat{\boldsymbol{i}}_{\boldsymbol{m}}$ at the steady state, as shown in Fig. 5. It should be noted that the variables in Fig. 5 are all the alternating quantities under $\alpha\beta$-stationary frame, which is different from the dc type in synchronous d-q frame. The steady-state $\boldsymbol{i}_1 - \hat{\boldsymbol{i}}_{\boldsymbol{m}}$ can be defined as $\hat{\boldsymbol{i}}_{\boldsymbol{t}}$, the estimated trust component of $\boldsymbol{i}_1$, which corresponds to I_q in secondary flux orientated control. When estimated secondary time constant $\hat{T}_2$ converges to real value, estimated magnetizing current $\hat{\boldsymbol{i}}_{\boldsymbol{m}}$ will approach the real one too.

Second, based on the analysis abovementioned, when only steady state is considered, the adaptive law (9) can be simplified as

$$\frac{1}{\hat{T}_2} = \left(K_p + \frac{1}{s}K_i\right)\boldsymbol{i_m}(\boldsymbol{i}_1 - \hat{\boldsymbol{i}}_{\boldsymbol{m}}). \tag{12}$$

As can be seen, the physical significance of (12) is clear now that the vertical relationship of $\boldsymbol{i_m}$ and $\boldsymbol{i}_1 - \hat{\boldsymbol{i}}_{\boldsymbol{m}}$ is utilized to represent the error of estimated secondary time constant. Besides, it is found that the coefficient L_2/L_m^2 in (4) has none influence on the steady-state value of secondary time constant identified by (9). However, the coefficient σL_1 also contains

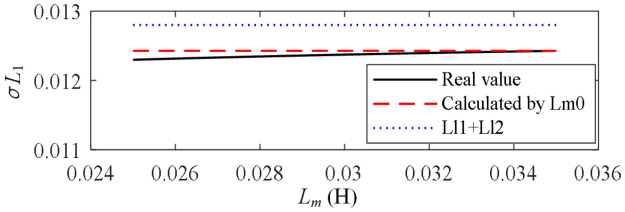

Fig. 6. Numeric analysis of the simplification.

magnetizing inductance, which can be rewritten as

$$\sigma L_1 = \left(1 - \frac{L_m^2}{L_1 L_2}\right) L_1 = L_{l1} + \frac{L_{l2} L_m}{L_{l2} + L_m}. \tag{13}$$

Considering that the secondary leakage inductance is relatively smaller than the primary leakage inductance and magnetizing inductance in LIMs, it can be deduced that the error of magnetizing inductance in (4) has a weak impact on the steady-state accuracy of secondary time constant identified by (9). In the conventional identification method for RIMs, the simplification of leakage coefficient is usually conducted as

$$\sigma L_1 = L_{l1} + L_{l2}. \tag{14}$$

However, different from that in RIMs, it is suggested to calculate the coefficient σL_1 by using the static value of magnetizing inductance in LIMs, defined as L_{m0}, to improve the accuracy as much as possible. It is the reflection of difference between RIMs and LIMs. The numeric comparison is shown in Fig. 6, in which two simplified calculation methods and the real value of coefficient σL_1 are given by adopting the prototype parameters in this article. As can be seen, by using the L_{m0}, the error is quite small even when the real magnetizing inductance deviates heavily from the static value. However, the other simplified method $L_{l1}+L_{l2}$ has a relatively large error all the time.

C. Static Stability Analysis

Although the global asymptotic stability of the secondary time constant identification system has been proved in Section III-A, the following analysis will explain why the stability range is extended with a more intuitive perspective. And comparation with the method discussed in [32] will be conducted, which is based on the results in Section III-B. That is the reason for splitting it from Section III-A and placing it after Section III-B.

First, the phase error between magnetizing current and estimated item in Fig. 5 is calculated by

$$\theta_{err} = \arctan\left(\frac{I_q}{I_d}\right) - \arctan\left(\frac{\hat{I}_q}{\hat{I}_d}\right) \tag{15}$$

where $I_{d,q}$ is the d- and q-axis components of primary current in secondary flux orientation synchronous d-q frame, corresponding to $\boldsymbol{i}_t$ and $\boldsymbol{i}_m$ in stationary reference frame.

Considering that the precise measured speed is adopted in the control system, it can be obtained that

$$\omega_1 - \omega_r = \omega_{sl} = \frac{I_q}{T_2 I_d} = \hat{\omega}_{sl} = \frac{\hat{I}_q}{\hat{T}_2 \hat{I}_d}. \tag{16}$$

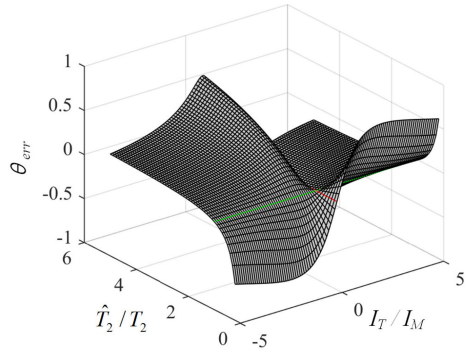

Fig. 7. Three-dimensional diagram for relationship of θ_{err} with $\hat{T}_2/T_2$ and I_q/I_d.

Combining (15) and (16), it will get

$$\theta_{err} = \arctan\left(\frac{I_q}{I_d}\right) - \arctan\left(\frac{\hat{T}_2}{T_2}\frac{I_q}{I_d}\right). \tag{17}$$

It is distinct that the phase error is influenced by both of identified secondary time constant and load condition I_q / I_d, as depicted in Fig. 7, in which the red line means the corresponding phase error under I_T / $I_M = 0$ and the green line means the corresponding phase error under correct estimated secondary time constant, that is to say, $\hat{T}_2/T_2 = 1$. As can be seen, under the two states, the phase error maintains as zero.

As shown in Fig. 7, the sign of phase error is divided into four parts by $I_q/I_d = 0$ and $\hat{T}_2/T_2 = 1$. That is to say, the relationship between phase error and identified secondary time constant can be flipped by the operation states.

According to Fig. 5, the adaptive law based on the cross product between ψ_r and $\hat{\psi}_r$ [32] can be rearranged to the similar form with (12) by using $\boldsymbol{i_m}$and $\hat{\boldsymbol{i}}_{\boldsymbol{m}}$, as described by

$$\varepsilon = i_{m\beta}\hat{i}_{m\alpha} - \hat{i}_{m\beta} i_{m\alpha} = -\left|\boldsymbol{i_m}\right| \left|\hat{\boldsymbol{i}}_{\boldsymbol{m}}\right| \sin\theta_{err}. \tag{18}$$

The identification system designed by (18) will lose efficacy under $I_q / I_d < 0$, such as the breaking condition. Despite that the sign of PI gains can be changed by judging the operation state online to extend the stable range, it will increase the complexity of system and may result in instability during mode switching process.

However, for the strategy based on (9), under steady state, it will get

$$\varepsilon' = \boldsymbol{i_m}\hat{\boldsymbol{i}}_t = \left|\boldsymbol{i_m}\right| \left|\hat{\boldsymbol{i}}_t\right| \cos\left(\frac{\pi}{2} \pm \theta_{err}\right) = \mp \left|\boldsymbol{i_m}\right| \left|\hat{\boldsymbol{i}}_t\right| \sin\theta_{err} \tag{19}$$

where "$\pm$" changes with the direction of thrust component of primary current automatically.

As a consequence, the adaptive mechanism (9) can maintain stability under all the operation range. It can be divided into two parts, one for steady state error and the other only the dynamic item, as illustrated by

$$\frac{1}{\hat{T}_2} = \left(K_p + \frac{1}{s}K_i\right) [\underbrace{\boldsymbol{i_m}(\boldsymbol{i}_1 - \hat{\boldsymbol{i}}_{\boldsymbol{m}})}_{\text{steady}} \underbrace{-\hat{\boldsymbol{i}}_{\boldsymbol{m}}(\boldsymbol{i}_1 - \hat{\boldsymbol{i}}_{\boldsymbol{m}})}_{\text{dynamic}}]. \tag{20}$$

IV. Parallel Identification Strategy for LIMs

A. Simplified Magnetizing Inductance Identification Method

Compared with resistance parameters, the difficulty of magnetizing inductance identification is relatively high. It is for the reason that the distribution of magnetizing inductance is quite wide in the mathematical model of IMs. The coupling problem will be one of the key points especially when the secondary parameter needs to be estimated simultaneously.

Different from the torque or reactive power, the quantities such as magnetizing current has two degrees of freedom, i.e., the amplitude and phase, which can be utilized to accomplish parallel identification. For the reason that there is no isolated magnetizing inductance in (5), it should be selected as the reference model on the premise of accurate secondary time constant for magnetizing inductance identification design. Defining the back EMF as $\boldsymbol{e_m}$, the voltage model (4) can be rearranged as

$$\boldsymbol{e_m}=\frac{L_m^2}{L_2}\frac{d\boldsymbol{i_m}}{dt}=\frac{\hat{L}_m^2}{\hat{L}_2}\frac{d\hat{\boldsymbol{i}}_{\boldsymbol{m}}}{dt}=\boldsymbol{u}_1-\left(R_1\boldsymbol{i}_1+\sigma L_1\frac{d\boldsymbol{i}_1}{dt}\right). \quad (21)$$

Considering the simplification (13), the back EMF can be calculated by the static value of magnetizing inductance. Combined (5) with (21), the identified magnetizing inductance can be obtained easily by solving

$$\frac{\hat{L}_m^2}{\hat{L}_2}=|\boldsymbol{e_m}|\,/\left|\frac{d\boldsymbol{i_m}}{dt}\right|. \quad (22)$$

However, it can be only established on the basis of known secondary time constant, that is to say, it should be applied with the identification of secondary time constant parallelly. Compared with the conventional online method [14], it has the superiorities that less simplifications are needed and no PI controller is used, which will improve the accuracy and portability to a large extent. Specially, the back EMF rather than the magnetizing current is utilized in (22), which can avoid the pure integrator problem. Correspondingly, the adaptive strategy of secondary time constant is modified as

$$\frac{1}{\hat{T}_2}=\left(K_p+\frac{1}{s}K_i\right)\frac{d\boldsymbol{\varepsilon_m^T}}{dt}\left(\frac{d\boldsymbol{i}_1}{dt}-\frac{d\hat{\boldsymbol{i}}_{\boldsymbol{m}}}{dt}\right). \quad (23)$$

As a result, the proposed dual-parameter identification is constructed on the derivatives of magnetizing current rather than the magnetizing current. The corresponding stability analysis is similar to the former content, as well as the physical significance. Besides, to avoid the dynamic influence of identified magnetizing inductance, the reference derivatives of magnetizing current in (23) can be calculated by the static value of magnetizing inductance, as illustrated by

$$\frac{d\boldsymbol{i_m}}{dt}=\frac{L_{20}}{L_{m0}^2}\boldsymbol{e_m}. \quad (24)$$

B. Decoupling Analysis of Parallel Identification

The coupling of parallel identification is usually neglected in some studies, which derive the adaptive laws separately. However, the dynamics will be affected with each other, which may lead to the difficulty in tuning of controllers or even stability problem. Whereas, in the proposed strategy, the coupling is relieved to some extent, which is one of the key contributions in this article. It can be discussed by parameter sensitivity analysis aspect.

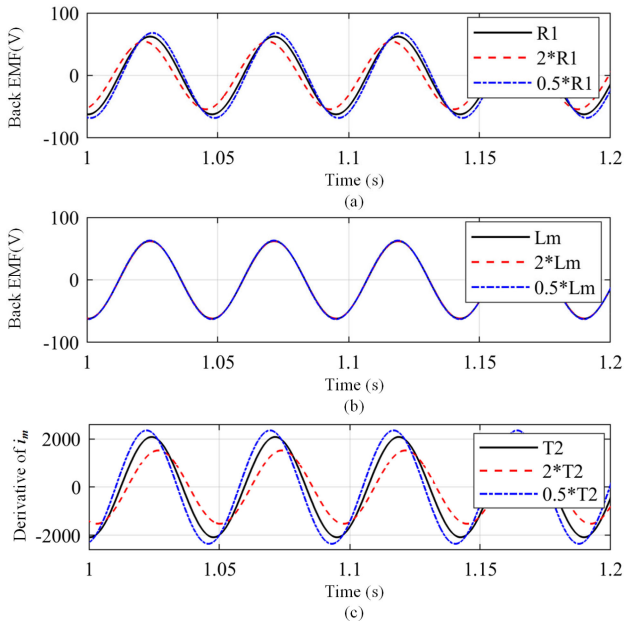

Fig. 8. Sensitivity analysis results of key parameters. (a) Primary resistance. (b) Magnetizing inductance. (c) Secondary time constant.

First of all, the analyzed parameter should be determined. Considering that the secondary resistance always appears with the secondary inductance in the mathematic model (11), it will be difficult to separate secondary resistance and magnetizing inductance. Thus, despite that the equation of secondary time constant contains the magnetizing inductance, it can be seen as one integrated independent parameter, just like that in the proposed identification system.

From the adopted voltage model (21) and current model (5), the error equation can be derived as

$$\Delta\boldsymbol{e_m}=-\left[\hat{R}_1\boldsymbol{i}_1+(\sigma L_1-\hat{\sigma}\hat{L}_1)\frac{d\boldsymbol{i}_1}{dt}\right] \quad (25)$$

$$\frac{d\Delta\boldsymbol{i_m}}{dt}=\omega_2\boldsymbol{J}\Delta\boldsymbol{i_m}-\left(\frac{1}{T_2}-\frac{1}{\hat{T}_2}\right)\boldsymbol{i_m}+\left(\frac{1}{T_2}-\frac{1}{\hat{T}_2}\right)\boldsymbol{i}_1. \quad (26)$$

As can be seen, the voltage model is mainly affected by leakage coefficient and primary resistance; the current model is only determined by secondary time constant. In the leakage coefficient as stated in (13), assuming that leakage inductance is known, it is mainly influenced by magnetizing inductance. The sensitivity analysis of the abovementioned three key parameters are illustrated in Fig. 8.

It can be found that the voltage model is sensitive to primary resistance but nearly independent with magnetizing inductance. When it comes to the current model, it is heavily influenced by the secondary time constant. Both

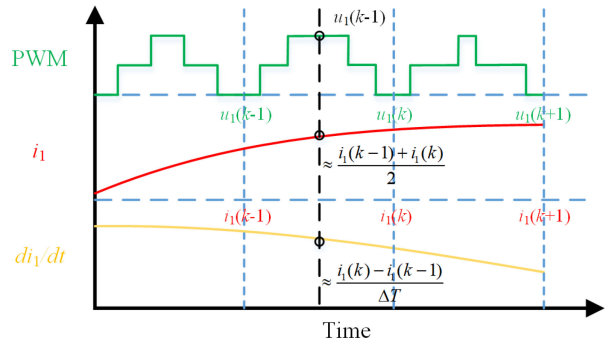

Fig. 9. Schematic diagram of discretization in reference model.

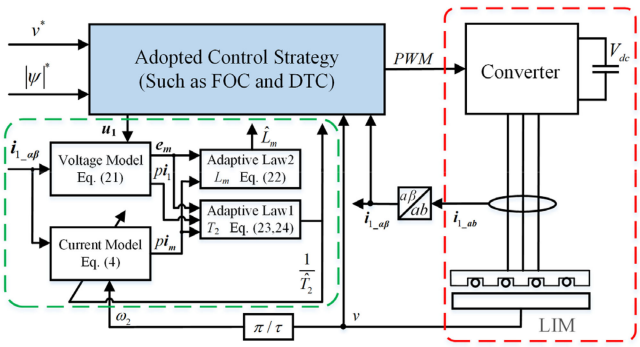

Fig. 10. Whole system of both control and parameter identification.

primary resistance and secondary time constant will result in the phase and amplitude error in estimated quantities distinctly.

Synthesizing the abovementioned theories and analytical results, it can be summarized that even if the precise magnetizing inductance has not been acquired, the voltage model can observe the back EMF precisely. Furthermore, the identified secondary time constant of adopted method can track the real value with small error. Then, on the basis of the converged secondary time constant, the accurate magnetizing inductance can be identified by (22). The overall stability is apparent, which is another superiority of the proposed method. As to the primary resistance, it can be set as the research target in the future work to eliminated the negative effects on estimation.

C. Realization in Digital System

Considering that the proposed identification method relies on the precise observation of selected quantities, which will heavily influence the performance, the suppression of discretization error in digital system should be put emphasis to improve the identification precision. Different from the compensation of inverter nonlinearity, it should be specially designed under different applications. Besides, as the primary voltage is usually reconstructed by the reference voltage rather than sampled, the delay time in voltage vector sequence should be considered. For the voltage model, considering that the derivatives of primary current need to be computed in (21), other variables should be synchronized with them, that is to say, half sample period should be delayed. As the natural delay exists between the reference voltage and real PWM waveform, the discrete form of (21) can be expressed as

$$\boldsymbol{e_m}\left(k-\frac{1}{2}\right)=\boldsymbol{u}_1(k-1)-\left(R_1\frac{\boldsymbol{i}_1(k-1)+\boldsymbol{i}_1(k)}{2}+\sigma L_1\frac{\boldsymbol{i}_1(k)-\boldsymbol{i}_1(k-1)}{\Delta T}\right) \tag{27}$$

where the k and k-1 represent the variables at the kth and the (k-1)th time steps, respectively, $\boldsymbol{e}_m(k\text{-}1/2)$ the discrete back EMF taking into consideration the effect of discretization error, and ΔT the sample period. It is presented visually in Fig. 9.

Correspondingly, in the current model, to balance the calculation time and accuracy, the improved Euler's method is adopted to obtain the discrete form of (5), as illustrated by

$$\begin{cases}\bar{\boldsymbol{i}}_{\boldsymbol{m}}(k)=\boldsymbol{i_m}(k-1)+[\omega_2\boldsymbol{J}\boldsymbol{i_m}(k-1)-\frac{1}{T_2}\boldsymbol{i_m}(k-1)\\ \qquad\qquad +\frac{1}{T_2}\boldsymbol{i}_1(k-1)]\Delta T\\ \boldsymbol{i'}_{\boldsymbol{m}}(k-\frac{1}{2})=\frac{1}{2}\{[\omega_2\boldsymbol{J}\boldsymbol{i_m}(k-1)-\frac{1}{T_2}\boldsymbol{i_m}(k-1)\\ \qquad\qquad +\frac{1}{T_2}\boldsymbol{i}_1(k-1)]\\ \qquad\qquad +[\omega_2\boldsymbol{J}\bar{\boldsymbol{i}}_{\boldsymbol{m}}(k)-\frac{1}{T_2}\bar{\boldsymbol{i}}_{\boldsymbol{m}}(k)+\frac{1}{T_2}\boldsymbol{i}_1(k)]\}\\ \boldsymbol{i_m}(k)=\boldsymbol{i_m}(k-1)+\boldsymbol{i'}_{\boldsymbol{m}}(k-\frac{1}{2})\Delta T\end{cases} \tag{28}$$

where $\bar{\boldsymbol{i}}_{\boldsymbol{m}}$ is the predicted magnetizing current in the first round, $\boldsymbol{i'}_{\boldsymbol{m}}(k-1/2)$ the discrete derivatives of magnetizing current taking into consideration the effect of discretization error.

From (28), the discrete derivatives of magnetizing current considering the effect of discretization error can be acquired directly, which is synchronized with the discrete derivatives of primary current and back EMF in (27).

D. Overall System Construction

Integrating the strategies abovementioned, the whole system that includes the parameter identification, control strategy, and main circuit is illustrated as Fig. 10. The identified parameters can be adopted in the control strategies to improve the performance if it is needed. It should be noted that for the proposed method is designed under stationary reference frame, it has no concern with the adopted control strategy. This is a prominent advantage compared with the methods based on the flux orientation, which can be only used in the FOC or should be reformed in some other strategies.

Fundamentally, the adopted identification method for secondary time constant relies on the angel information between magnetizing current $\boldsymbol{i}_m$ and thrust current $\boldsymbol{i}_t$. And the identification of magnetizing inductance utilizes the amplitude information between back EMF $\boldsymbol{e}_m$ and magnetizing current $\boldsymbol{i}_m$. As a result, although the adopted MRAS is a relatively conventional algorithm, the proposed identification method can realize the following distinctive properties, which are the main contributions of this article:

TABLE II
DIFFERENCES AND OBSTACLES FROM RIMS TO LIMS

Terms	RIM	LIM	Problem and solution
Parameter relationship	$L_m \gg L_{l1}$ $L_m \gg L_{l2}$	$L_m > L_{l1}$ $L_{l1} > L_{l2}$	Require for accuracy is larger; simplification should be careful
Simplification method	σL_1 $\approx L_{l1}+L_{l2}$ is adequate	σL_1 $\approx L_{l1}+L_{l2}$ leads to error	New simplification method is proposed and it is quite practical
Model	Mature model	Several kinds of models	Difficulty will be affected by model
Impact mechanism	L_m is mainly affected by saturation	LEE has large impact on L_m and R_2	Multiple factors make offline identification difficult and insufficient

TABLE III
MAIN PARAMETERS OF TWO AIMS

Name	Symbol	Value and Unit
Primary pole pitch length	τ	0.1485 m
Primary length	l	1.3087 m
Primary leakage inductance	L_{l1}	9 mH
Secondary leakage inductance	L_{l2}	3.8 mH
Mutual inductance	L_m	35 mH
Primary resistance	R_1	1.06 Ω
Secondary resistance	R_2	2.4 Ω

1) magnetizing inductance and secondary time constant are selected as the targets, which is unusual in parameter identification;
2) clear physical significance;
3) pure integrator is eliminated;
4) only one coefficient simplification is needed, which can better ensure the precision of identification;
5) weak coupling, firstly secondary time constant and then magnetizing inductance are identified successively;
6) only one PI controller is utilized, the workload of parameter tuning is light.

Finally, to reflect the differences between RIMs and LIMs, the corresponding obstacles in the research are summarized in Table II. As can be seen, there are much more challenges in the parameter estimation of LIMs.

V. SIMULATION AND EXPERIMENTAL RESULTS

Main parameters used in the validation are presented in Table III, which come from one prototyped LIMs platform, as shown in Fig. 11. Two coupled arc induction motors (AIMs) with large enough radius are used to simulate the properties of an actual LIMs [38]. One of the AIM is utilized as the drive motor and the other can be adopted as the load motor to produce negative thrust. However, in this way, the thrust cannot be directly measured by the torque transducer on the shaft. To satisfy some conditions that need the information of output torque, the extra permanent magnet synchronous motor based load producer is constructed.

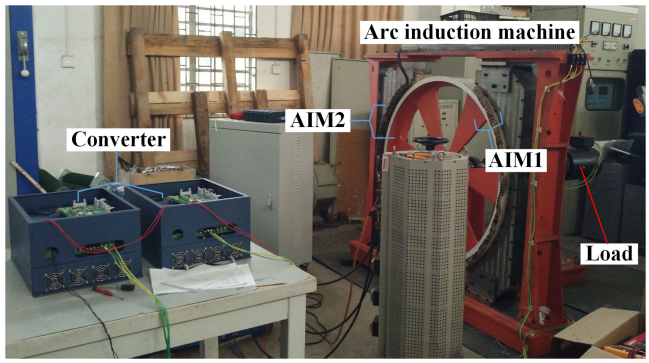

Fig. 11. LIMs test platform comprised of two AIMs.

The FOC is employed as the main control structure here to conduct the simulations and experiments. The comparative results of secondary time constant estimated by the cross product between secondary flux and estimated item [32] (called conventional method here) and the proposed dual-parameter online identification strategy are displayed to enhance the persuasion of effectiveness and superiority. Besides, the simplified scheme that omits the dynamic compensation part is also employed to illustrate the validity of physical significance analysis. In addition, to enhance comparability of different adaptive laws, the conventional method is adjusted as the form of angle error between reference and estimated derivatives of magnetizing current. The modified conventional and simplified adaptive laws are expressed as

$$\begin{cases} \varepsilon_{Con} = \frac{di_{m\beta}}{dt}\frac{d\hat{i}_{m\alpha}}{dt} - \frac{di_{m\alpha}}{dt}\frac{d\hat{i}_{m\beta}}{dt} \\ \varepsilon_{Sim} = \frac{di_{m\alpha}}{dt}\left(\frac{di_{1\alpha}}{dt} - \frac{d\hat{i}_{m\alpha}}{dt}\right) + \frac{di_{m\beta}}{dt}\left(\frac{di_{1\beta}}{dt} - \frac{d\hat{i}_{m\beta}}{dt}\right). \end{cases} \tag{29}$$

A. Simulation and Analysis

To reflect the influence of end effects on magnetizing inductance and secondary time constant in LIMs to simulate the real condition, the two parameters change with the rule of LEE factor $f(Q)$ [19] and $R_{2N}\times(1+0.04\times\text{abs}(\omega))$, respectively, for convenience. Besides, the PI controllers of three secondary time constant identification approaches are tuned to be the same for the similar form.

Firstly, the typical operation condition is conducted, in which the speed changes from 0→4→11→6 m/s at 0, 4, and 8 s, respectively, and load changes from 50→150→100 *N* at 2 and 6 s, respectively, as shown in Fig. 12. It can be seen that the estimated secondary time constant and magnetizing inductance by the proposed, simplified and conventional methods can all track the real values with fast dynamic response and precise steady state. To be more clearly, the detail drawings are given out, from which it can be concluded that 1) both the dynamic response and steady state are similar for the proposed and conventional methods; 2) the difference between the proposed and simplified methods mainly lies on the dynamic response,

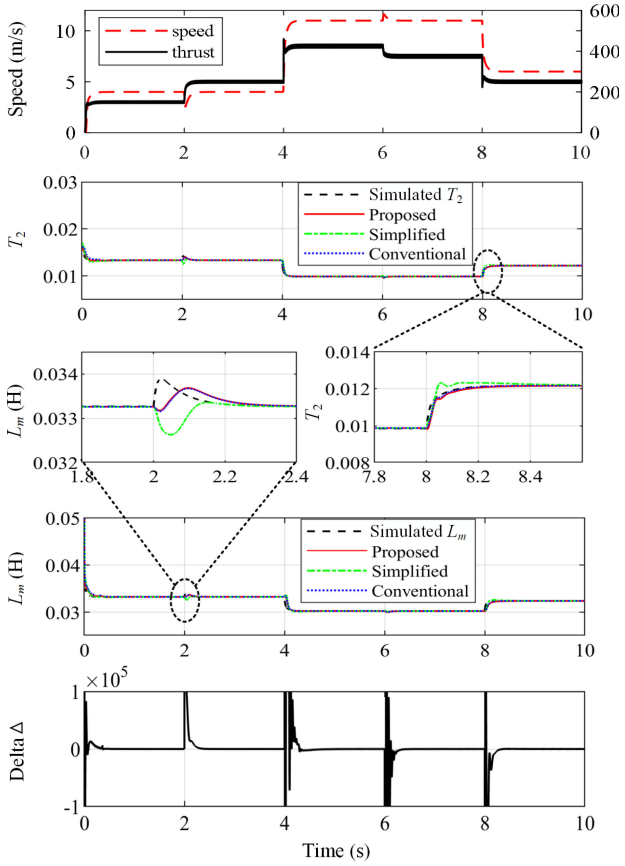

Fig. 12. Comprehensive simulation results of parameter identification for proposed, simplified and conventional methods with speed and load change.

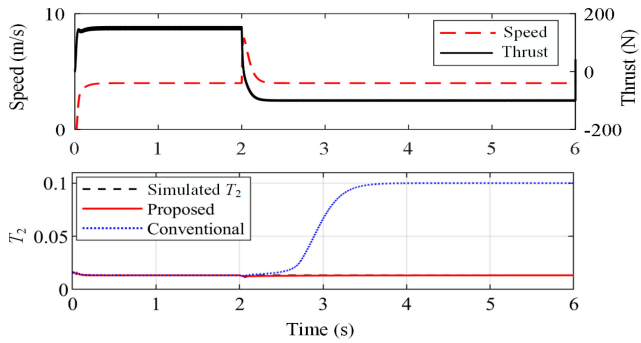

Fig. 13. Simulation results for the stability test.

which is consistent with the theory analyzed before. The second part of (20) just influences the dynamic performance. In the bottom of Fig. 12, "Delta Δ" just represents the simplified part, which is obtained by adopting the simplified method. As can be seen, it maintains as zero at steady state despite that it is not used in the adaptive law.

Considering the stability problem of conventional method, the experiment is specially designed to make verification, in which the LIMs operate on the state of negative thrust under positive speed to make $i_q / i_d < 0$. The results are shown in Fig. 13. As can be seen, the estimated secondary time constant by conventional

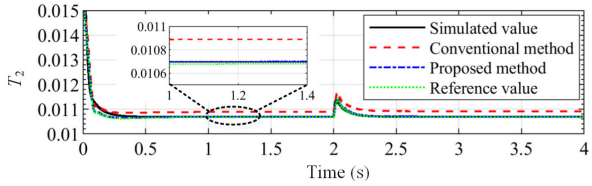

Fig. 14. Simulation result for verifying the decoupling analysis.

method is divergent after 2 s. However, the adaptive law derived by Popov's criterion for hyperstability is stable under the same state.

In Section III-B, a vital simplification is made for (13), which will heavily influence the precision if it is not correct. To further test the difference between the two simplification methods, the comparative simulation results are shown as Fig. 14, in which the speed is set as 9 m/s and load changes at 2 s. Three different operation conditions are conducted: 1) with conventional simplification method by (14); 2) with proposed simplification method; 3) with real coefficients as the reference value. Besides, the simulated value of secondary time constant is illustrated as the standard value. As can be seen, with the adopted simplification method, the unwanted identification error in secondary time constant has been largely eliminated to an acceptable value. Although the thought is relatively intuitionistic, it is a quite practical method that would not increase the complexity and calculation burden.

Besides, from Fig. 14, the decoupling analysis in Section IV-B can be verified too. As can be seen, except for the condition under the conventional simplification method, the other three results are very closed. That is to say, the proposed simplification method is necessary and sufficient to ensure the requirements for accuracy of identification. After the secondary time constant is determined, the current model can play the role of reference model to provide the magnitude information for magnetizing inductance identification. In this way, the coupling of the dual-parameters identification can be removed well.

Finally, to test the importance of discretization method, the comparison results between conventional forward Euler's method and the adopted improved Euler's method are illustrated in Fig. 15. Four different modes are set as follows:

1) both voltage and current model use the improved Euler's method;
2) only voltage model uses the improved Euler's method;
3) only current model uses the improved Euler's method;
4) both voltage and current model use the conventional forward Euler's method.

It is worth mentioning that the simulation model of control and identification system is fully discretized to make it more similar to the real digital real-time system. As can be seen, only by utilizing the discretization equation in (27) and (28), the identified parameters can track the simulated values with very small error. It can be concluded that the proposed method is very sensitive to the observe error and the special design of discretization structure is essential for obtaining correct value.

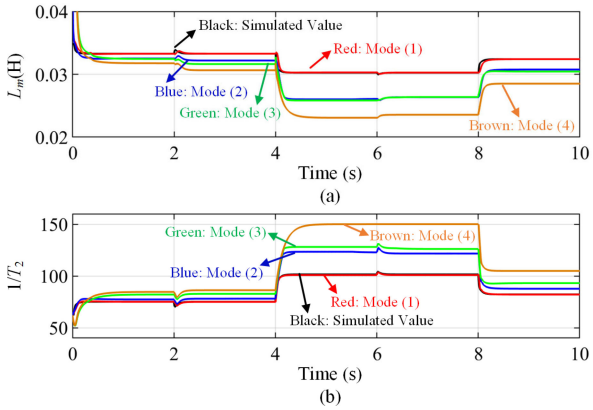

Fig. 15. Simulation result of identification parameters by four different discretization modes. (a) Magnetizing inductance. (b) Inverse of Secondary time constant.

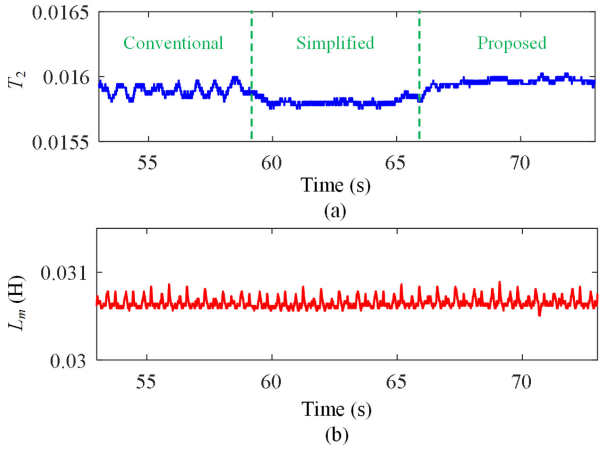

Fig. 17. Experimental results of the dynamic switching state. (a) Secondary time constant. (b) Magnetizing inductance.

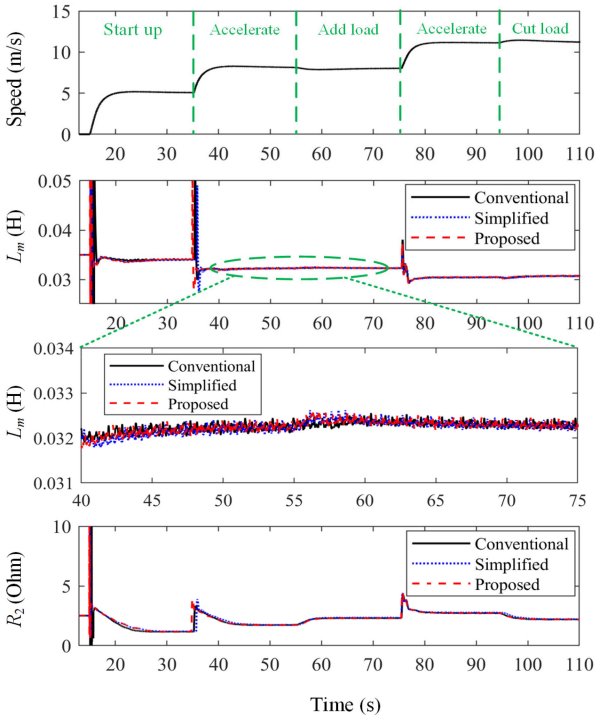

Fig. 16. Experimental results of parameter identification for the proposed, simplified and conventional methods with changing speed and load.

B. Experimental Results and Analysis

As the accuracy of reconstructed voltage in the digital experiment system is important to the proposed identification strategy, one practical compensation method for power inverter nonlinearity is adopted to suppress the influence of error in voltage signal [37] without using complex coefficients of inverter, such as turn-ON and turn-OFF delay time. Similar to the simulation, the comprehensive experiments with accelerating and load change are conducted first, as shown in Fig. 16. As can be seen, the parameter identification system can start with the LIMs control system, in which the transient fluctuation appears. To avoid the negative impacts, when it is adopted in compensation, it can be filtered by a low-pass filter.

It is clear that in Fig. 16, the identified steady-state magnetizing inductance, secondary resistance, and secondary time constant of three different adaptive laws are nearly the same under various speed and load states. Besides, the trends follow the functional rule of end effects on the parameters. For the magnetizing inductance, it can be noted that the online identified value is very close to the offline one without the unstable condition. As to secondary resistance, the relatively distinct variation under load change is determined by both end effects and the skin effect on secondary side for the varying of slip frequency. It is difficult to derive the integral change rule of secondary resistance by theoretical study, which considers all of the main factors, and it makes the online identification more important. The steady-state values of three different methods are nearly the same, which is consistent with the theoretical analysis and simulation results. And the difference on the dynamic process is quite small. It indicates that the dynamic part of (20) has little influence on the overall control performance, especially the steady state. In Fig. 17, the dynamic switching of three different methods is accomplished at 11 m/s. It is further confirmed that the three methods have the similar property for smooth transition and almost the same steady-state value especially for the magnetizing inductance identification.

To compare the stability of proposed and conventional methods, the experiment of relatively long-time decelerating condition is conducted to produce the state of $i_q / i_d < 0$ during the dynamic process. The corresponding results are shown as Fig. 18. It can be seen that both methods are stable when the speed accelerates from 5 to 11 m/s. However, under the transient process of deceleration from 11 to 5 m/s, the conventional method turns instable with the estimated secondary time constant oscillating heavily. For the proposed method, despite that the dynamic response is relatively slow, the stability can be always maintained in the whole process.

The steady-state values of identified parameters under different motor speeds are displayed in Fig. 19. It can be seen that the

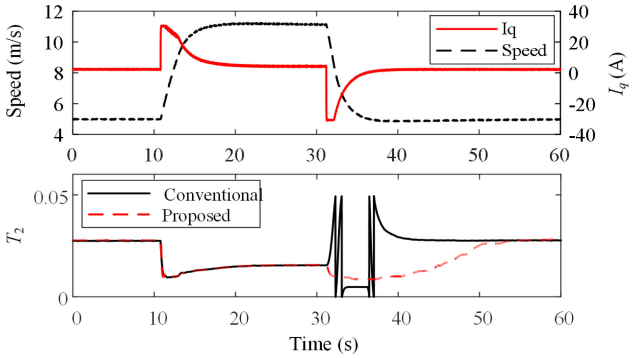

Fig. 18. Experimental results of the stability comparison.

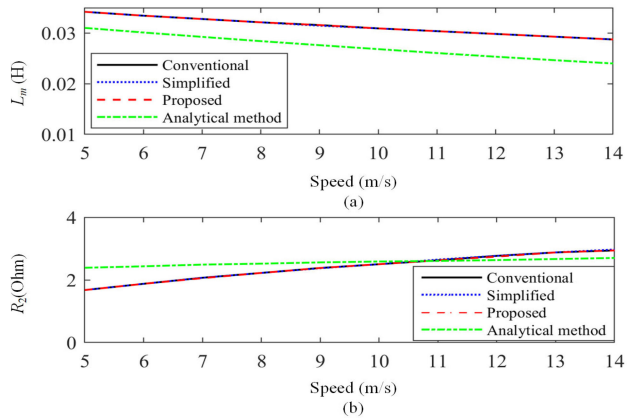

Fig. 19. Experimental results of the identified parameters under different speeds. (a) Magnetizing inductance. (b) Secondary resistance.

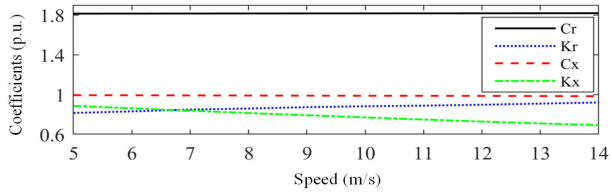

Fig. 20. Circuit calculation results of modification coefficients in LIMs.

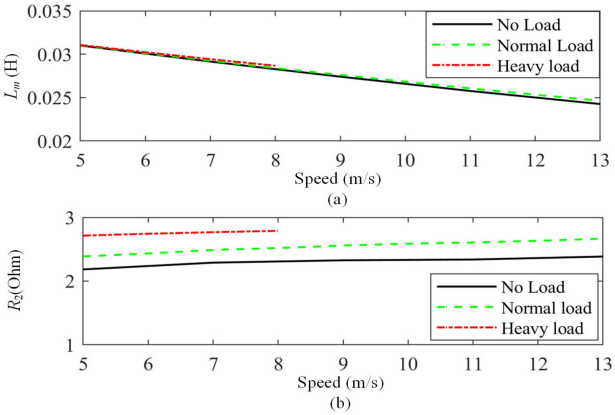

Fig. 21. Comparison of parameters by analytical method under different load conditions. (a) Magnetizing inductance. (b) Secondary resistance.

overall trend, variation range, and gradient of identified parameters are consistent with relevant theoretical research. All of the identified parameters have quite a wide change with the speed. Specifically, taking the magnetizing inductance as example, the variation from 5 to 15 m/s is 0.006 H (about 17% of the static value), which just mainly comes from the increase of speed. When the load condition and saturation degree change greatly, the range of variation in parameters may be further extended. It indicates that the parameter identification is crucial for the LIMs and has potential application in the high-performance strategies, which are dependent of accurate parameters, such as model predictive control, loss minimization control, and so on. Although the identification results of three methods are nearly the same in Figs. 16 and 17, It is for the reason that there is no unstable condition in these tests. The similarity just reflects the uniformity of the three different methods, which will be helpful to build up one unified framework.

The abovementioned analysis of experiments mainly focuses on the comparation with the offline identified values and overall trend of theoretical research. To verify the effectiveness of identification results in the experiments quantitatively, the analytical method proposed in [18] is utilized to calculate the modified value of estimated parameters considering the end effects. As stated in Fig. 1, four coefficients are introduced to modify the magnetizing inductance and secondary resistance.

By injecting the speed and slip frequency measured through experiments, the four coefficients can be calculated, as shown in Fig. 20. Then, the quantitative comparison can be drawn as Fig. 19. As can be seen, not only is the trend of analytical results coincident with the experimental results, but also the specific value is very closed. The difference may come from the other factors in parameters change, such as saturation, skin effect, and temperature. It is quite difficult to consider all of them in the theoretical analysis, for which the online identification will be more useful. Besides, it is worth mentioning that the error in other parameters, such as primary resistance, will affect the precision of identification results to some extent. The method to solve this problem can be set as the research goals in the future work.

Furthermore, the aforementioned verification mainly focuses on the discussion of speed factor in the end effects. The other important issue is the slip frequency, which can be adjusted by changing the load condition with constant speed. The comparisons of analytical results under different load conditions are illustrated in Fig. 21. As can be seen, changing in slip frequency by adding loads has a relatively small influence on the value of magnetizing inductance. However, when it comes to the secondary resistance, the variation is apparent during the whole speed range. From the experimental results in Fig. 16, it can be seen that the identified magnetizing inductance slightly increases and identified secondary resistance rises largely when the load

is added, which is just the same as that in the results of analytical method.

From the abovementioned verification method, the effectiveness of experimental results in identified parameters can be assured to some extent, not only from the key points and overall trend aspects, but also from the quantitative perspective by analytical method. From another side, the online identification in this article has just verified the validity of theoretical research started from the design of LIMs.

VI. Conclusion

In this article, one practical online dual-parameter identification strategy for LIMs is proposed to solve the severe deviation of magnetizing inductance and secondary time constant, which are affected by multiple nonlinear factors. Main contributions and analysis results are briefly summarized as follows.

1) The physical significance and static stability of secondary time constant adaptive law derived by Popov's criterion for hyperstability are clarified detailly, which is based on the mathematic model with magnetizing current as state variable and inverse-Γ dynamic circuit.
2) According to specificity of parameters in LIMs, one improved simplification method is presented to reduce the estimation error and only one coefficient is involved, which is effective but would not increase the complexity.
3) Based on the works abovementioned, the magnetizing inductance estimation method is proposed to form the dual-parameter identification system with only one PI controller,
4) The coupling in the estimation of two parameters is weak. Specifically, first, secondary time constant and then magnetizing inductance are estimated successively.
5) By changing the state variable from magnetizing current to derivative of magnetizing current, pure integrator is eliminated and new adaptive laws are derived.
6) Suitable discrete equations of voltage and current model are fully derived to reduce the influence of delay time in voltage vector sequence and discretization error.
7) The proposed method and simplified method by ignoring the dynamic part are found to have the similar property with the method based on the cross product between real and estimated fluxes, which can be unified to the same framework except for the braking state.
8) The online identified parameters can follow the theory of end effects under different operation conditions and basically match the offline identified values.

Besides, the proposed method can be also extended to some applications of rotary induction motor, which have relatively high demands on accuracy of parameters, such as electric vehicle situation.

References

[1] W. Xu, R. Islam, and M. Pucci, *Advanced Linear Machines and Drive Systems*. Singapore: Springer, Sep. 2019.

[2] I. Boldea, L. Tutelea, W. Xu, and M. Pucci, "Linear electric machines, drives and MAGLEVs: An overview," *IEEE Trans. Ind. Electron.*, vol. 65, no. 9, pp. 7504–7515, Sep. 2018.

[3] J. Zou, W. Xu, X. Yu, Y. Liu, and C. Ye, "Multistep model predictive control with current and voltage constraints for linear induction machine based urban transportation," *IEEE Trans. Veh. Technol.*, vol. 66, no. 12, pp. 10817–10829, Dec. 2017.

[4] D. Hu, W. Xu, R. Dian, and Y. Liu, "Loss minimization control strategy for linear induction machine in urban transit considering normal force," *IEEE Trans. Ind. Appl.*, vol. vol. 55, no. 2, pp. 1536–1549, Mar./Apr. 2019.

[5] R. Dian, W. Xu, J. Zhu, D. Hu, and Y. Liu, "An improved speed sensorless control strategy for linear induction machines based on extended state observer for linear metro drives," *IEEE Trans. Veh. Technol.*, vol. 67, no. 10, pp. 9198–9210, Oct. 2018.

[6] F. Alonge, M. Cirrincione, F. D'Ippolito, M. Pucci, and A. Sferlazza, "Parameter identification of linear induction motor model in extended range of operation by means of input-output data," *IEEE Trans. Ind. Appl.*, vol. 50, no. 2, pp. 959–972, Mar./Apr. 2014.

[7] A. Accetta, M. Cirrincione, M. Pucci, and A. Sferlazza, "State-space vector model of linear induction motors including end-effects and iron losses—Part II: Model identification and results," *IEEE Trans. Ind. Appl.*, vol. 56, no. 1, pp. 245–255, Jan./Feb. 2020.

[8] G. Kang, J. Kim, and K. Nam, "Parameter estimation scheme for low-speed linear induction motors having different leakage inductances," *IEEE Trans. Ind. Electron.*, vol. 50, no. 4, pp. 708–716, Aug. 2003.

[9] Z. Zhang, T. R. Eastham, and G. E. Dawson, "Peak thrust operation of linear induction machines from parameter identification," in *Proc. Conf. Rec. IEEE Ind. Appl. Conf. 30th IAS Annu. Meeting*, 1995, vol. 1, pp. 375–379.

[10] L. Shi, K. Wang, and Y. Li, "On-line parameter identification of linear induction motor based on adaptive observer," in *Proc. Int. Conf. Elect. Mach. Syst.*, 2007, pp. 1606–1609.

[11] X. Qiwei, S. Cui, Q. Zhang, L. Song, and X. Li, "Research on a new accurate thrust control strategy for linear induction motor," *IEEE Trans. Plasma Sci.*, vol. 43, no. 5, pp. 1321–1325, May 2015.

[12] J. Ren and Y. Li, "MRAS based online magnetizing inductance estimation of linear induction motor," in *Proc. Int. Conf. Elect. Mach. Syst.*, Seoul, South Korea, 2007, pp. 1580–1583.

[13] E. Levi and M. Wang, "Online identification of the mutual inductance for vector controlled induction motor drives," *IEEE Trans. Energy Convers.*, vol. 18, no. 2, pp. 299–305, Jun. 2003.

[14] L. Liu, Y. Guo, and J. Wang, "Online identification of mutual inductance of induction motor without magnetizing curve," in *Proc. Annu. Amer. Control Conf.*, Milwaukee, WI, USA, 2018, pp. 3293–3297.

[15] M. Ranta and M. Hinkkanen, "Online identification of parameters defining the saturation characteristics of induction machines," *IEEE Trans. Ind. Appl.*, vol. 49, no. 5, pp. 2136–2145, Sep./Oct. 2013.

[16] B. Karanayil, M. F. Rahman, and C. Grantham, "An implementation of a programmable cascaded low-pass filter for a rotor flux synthesizer for an induction motor drive," *IEEE Trans. Power Electron.*, vol. 19, no. 2, pp. 257–263, Mar. 2004.

[17] A. Rafiq, M. G. Sarwer, M. Datta, and B. C. Ghosh, "Fast speed response field-orientation control induction motor drive with adaptive neural integrator," in *Proc. IEEE Int. Conf. Ind. Technol.*, 2005, pp. 610–614.

[18] W. Xu *et al.*, "Equivalent circuits for single-sided linear induction motors," *IEEE Trans. Ind. Appl.*, vol. 46, no. 6, pp. 2410–2423, Nov./Dec. 2010.

[19] J. Duncan, "Linear induction motor-equivalent-circuit model," *Proc. Inst. Elect. Eng.*, vol. 130, no. 1, pp. 51–57, Jan. 1983.

[20] W. Xu, J. Zhu, Y. Zhang, Y. Li, Y. Wang, and Y. Guo, "An improved equivalent circuit model of a single-sided linear induction motor," *IEEE Trans. Veh. Technol.*, vol. 59, no. 5, pp. 2277–2289, Jun. 2010.

[21] M. Pucci, "State space-vector model of linear induction motors," *IEEE Trans. Ind. Appl.*, vol. 50, no. 1, pp. 195–207, Jan./Feb. 2014.

[22] T. M. Rowan, R. J. Kerman, and D. Leggate, "A simple on-line adaption for indirect field orientation of an induction machine," *IEEE Trans. Ind. Appl.*, vol. 27, no. 4, pp. 720–727, Jul./Aug. 1991.

[23] L. Zhao, J. Huang, J. Chen, and M. Ye, "A parallel speed and rotor time constant identification scheme for indirect field oriented induction motor drives," *IEEE Trans. Power Electron.*, vol. 31, no. 9, pp. 6494–6503, Sep. 2016.

[24] F. L. Mapelli, A. Bezzolato, and D. Tarsitano, "A rotor resistance MRAS estimator for induction motor traction drive for electrical vehicles," in *Proc. Int. Conf. Elect. Mach.*, Marseille, France, Sep. 2012, pp. 823–829.

[25] X. Yu, M. W. Dunnigan, and B. W. Williams, "A novel rotor resistance identification method for an indirect rotor flux-orientated controlled induction machine system," *IEEE Trans. Power Electron.*, vol. 17, no. 3, pp. 353–364, May 2002.

[26] P. Cao, X. Zhang, S. Yang, Z. Xie, and Y. Zhang, "Reactive-power-based MRAS for online rotor time constant estimation in induction motor drives," *IEEE Trans. Power Electron.*, vol. 33, no. 12, pp. 10835–10845, Dec. 2018.
[27] S. Maiti, C. Chaakraborty, Y. Hori, and M. C. Ta, "Model reference adaptive controller-based rotor resistance and speed estimation techniques for vector controlled induction motor drive utilizing reactive power," *IEEE Trans. Ind. Electron.*, vol. 55, no. 2, pp. 594–601, Feb. 2008.
[28] F. Lin, H. Su, and H. Chen, "Induction motor servo drive with adaptive rotor time-constant estimation," *IEEE Trans. Aerosp. Electron. Syst.*, vol. 34, no. 1, pp. 224–234, Jan. 1998.
[29] P. Cao, X. Zhang, and S. Yang, "A unified-model-based analysis of MRAS for online rotor time constant estimation in an induction motor drive," *IEEE Trans. Ind. Electron.*, vol. 64, no. 6, pp. 4361–4371, Jun. 2017.
[30] K. Wang, B. Chen, G. Shen, W. Yao, K. Lee, and Z. Lu, "Online updating of rotor time constant based on combined voltage and current mode flux observer for speed-sensorless AC drives," *IEEE Trans. Ind. Electron.*, vol. 61, no. 9, pp. 4583–4593, Sep. 2014.
[31] D. P. Marcetic and S. N. Vukosavic, "Speed-sensorless AC drives with the rotor time constant parameter update," *IEEE Trans. Ind. Electron.*, vol. 54, no. 5, pp. 2618–2625, Oct. 2007.
[32] S. Yang, D. Ding, X. Li, Z. Xie, X. Zhang, and L. Chang, "A novel online parameter estimation method for indirect field oriented induction motor drives," *IEEE Trans. Energy Convers.*, vol. 32, no. 4, pp. 1562–1573, Dec. 2017.
[33] A. B. Proca and A. Keyhani, "Sliding-mode flux observer with online rotor parameter estimation for induction motors," *IEEE Trans. Ind. Electron.*, vol. 54, no. 2, pp. 716–723, Apr. 2007.
[34] J.-W. Choi and S.-K. Sul, "Inverter output voltage synthesis using novel dead time compensation," *IEEE Trans. Power Electron.*, vol. 11, no. 2, pp. 221–227, Mar. 1996.
[35] C. Choi, K. Cho, and J. Seok, "Inverter nonlinearity compensation in the presence of current measurement errors and switching device parameter uncertainties," *IEEE Trans. Power Electron.*, vol. 22, no. 2, pp. 576–583, Mar. 2007.
[36] D. Park and K. Kim, "Parameter-independent online compensation scheme for dead time and inverter nonlinearity in IPMSM drive through waveform analysis," *IEEE Trans. Ind. Electron.*, vol. 61, no. 2, pp. 701–707, Feb. 2014.
[37] Y. Park and S. Sul, "A novel method utilizing trapezoidal voltage to compensate for inverter nonlinearity," *IEEE Trans. Power Electron.*, vol. 27, no. 12, pp. 4837–4846, Dec. 2012.
[38] A. Majumdar and T. K. Bhattacharya, "Comparison of force developed in a linear induction machine and an equivalent arc linear induction machine at zero velocity," in *Proc. IEEE Int. Conf. Power Electron., Drives Energy Syst.*, 2018, pp. 1–5.

Dinghao Dong (Student Member, IEEE) received the B.E. degree in electrical engineering from Wuhan University, Wuhan, China, in 2017. He is currently working toward the Ph.D. degree with the School of Electrical Engineering, Huazhong University of Science and Technology, Wuhan, China.

His current research interests include control of brushless doubly fed induction generators, parameter identification, and control of linear induction motors.

Wei Xu (Senior Member, IEEE) received the double B.E. and M.E. degrees from Tianjin University, Tianjin, China, in 2002 and 2005, and the Ph.D. degree from the Institute of Electrical Engineering, Chinese Academy of Sciences, Beijing, China, in 2008, respectively, all in electrical engineering.

From 2008 to 2012, he was a Postdoctoral Fellow with the University of Technology Sydney, Vice Chancellor Research Fellow with the Royal Melbourne Institute of Technology, Japan Science Promotion Society Invitation Fellow with Meiji University, respectively. Since 2013, he has been Full Professor with State Key Laboratory of Advanced Electromagnetic Engineering in Huazhong University of Science and Technology, China. His research interests include design and control of linear/rotary machines.

Prof. Xu is a Fellow with the Institute of Engineering and Technology. He is the General Chair for 2021 International Symposium on Linear Drives for Industry Applications and 2023 IEEE International Conference on Predictive Control of Electrical Drives and Power Electronics, Wuhan, China. He has been Associate Editor for several leading IEEE Transactions Journals, such as IEEE TRANSACTIONS ON INDUSTRIAL ELECTRONICS, IEEE TRANSACTIONS ON VEHICULAR TECHNOLOGY, and IEEE TRANSACTIONS ON ENERGY CONVERSION.

Xinyu Xiao received the B.E. degree in electrical engineering from Hunan University, Changsha, China, in 2016. He is currently working toward the Ph.D. degree with the School of Electrical and Electronic Engineering, Huazhong University of Science and Technology, Wuhan, China.

His research interests include design and control of linear induction machines.

Yirong Tang (Student Member, IEEE) received the B.E. degree in electrical engineering in 2020 from the Huazhong University of Science and Technology, Wuhan, China, where he is currently working toward the Ph.D. degree with the State Key Laboratory of Advanced Electromagnetic Engineering and Technology.

His research interests include advanced control methods for permanent magnet synchronous machines, linear induction machines, and drives.

Kai Yang was born in Hubei, China, in 1976. He received the B.S., M.S., and Ph.D. degrees in electrical and electronic engineering from Huazhong University of Science and Technology, Wuhan, China, in 1998, 2000, and 2003, respectively.

He is currently a Professor and the Associate Dean with the School of Electrical and Electronic Engineering, Huazhong University of Science and Technology. His research interests include electrical engineering, utilization of new energy resources, and functional material actuators.